Applied Physics Express

LETTERS

6 kW/cm^2 UVC laser threshold in optically pumped lasers achieved by controlling point defect formation

To cite this article: Ronny Kirste *et al* 2018 *Appl. Phys. Express* **11** 082101

Applied Physics Express **11**, 082101 (2018)
https://doi.org/**10.7567/APEX.11.082101**

6 kW/cm^2 UVC laser threshold in optically pumped lasers achieved by controlling point defect formation

Ronny Kirste[1,2], Qiang Guo[1], J. Houston Dycus[1], Alexander Franke[1], Seiji Mita[1,2], Biplab Sarkar[1], Pramod Reddy[1,2], James M. LeBeau[1], Ramon Collazo[1], and Zlatko Sitar[1,2]

[1]*Department of Materials Science and Engineering, North Carolina State University, Raleigh, NC 27695-7919, U.S.A.*
[2]*Adroit Materials, 2054 Kildaire Farm Road, Suite 205, Cary, NC 27518, U.S.A.*

Received June 22, 2018; accepted July 10, 2018; published online July 27, 2018

Optically pumped lasing from AlGaN/AlN multiple quantum wells grown on single-crystalline AlN substrates with lasing thresholds as low as 6 kW/cm^2 is demonstrated via the reduction of unintentional point defects in the active region and waveguide, which reduces the non-radiative recombination by 2 orders of magnitude. A higher lasing threshold of 11 kW/cm^2 is observed for AlGaN barriers, owing to the reduced localization of electrons and holes in the wells. It is shown that for electrically injected UVC laser diodes, AlGaN barriers are essential.

Electrically injected AlGaN-based UVC laser diodes are widely desired for application in spectroscopy, non-line-of-sight communication, and biosensing.[1,2] Thus far, optically pumped lasing in the UVC range has been demonstrated by several groups using both sapphire and AlN substrates.[3–9] The achieved laser thresholds range from approximately 50 kW/cm^2 to several MW/cm^2. The differences in the laser threshold mainly arise from high point defect concentration due to unfavorable growth conditions, as well as high dislocation density in the case of growth on non-native substrates.[10–12] Additionally, the design of the multiple quantum well (MQW) structure influences the performance of the optically pumped lasers.[13] Understanding and controlling all these parameters to achieve the lowest possible laser threshold and highest possible internal quantum efficiency (IQE) is crucial for achieving electrically injected lasing. Among others, the performance of MQWs is impacted by (1) the Al content in the wells and barriers; (2) the thickness of the wells and barriers; (3) the number of QWs; and (4) the quality of the MQW structure, with regard to the homogeneity and interfacial roughness.[14] However, despite many demonstrations of optically pumped lasing in the UV range, little is known about the impact of the MQW design parameters on the laser threshold.

In this study, 6 kW/cm^2 threshold UVC lasing is demonstrated via a reduction of the point defect concentration in the waveguide and in the MQW. The distinction between the design of optically pumped and electrically driven laser structures, as they must satisfy different requirements, is discussed.

Optically pumped lasers were grown via metalorganic chemical vapor deposition on single-crystalline physical vapor transport grown AlN substrates.[3,15–17] First, a homoepitaxial AlN layer of approximately 200 nm thickness was grown. Next, a 150-nm-thick AlGaN waveguide with an Al content of 65% was deposited, followed by a 3× AlGaN/AlGaN MQW (2.5 nm/2.5 nm). The Al content in the wells for all the investigated samples was 55% for a targeted emission of approximately 265 nm, and the Al content in the barriers was varied from 60 to 100%. The structure was finished by a 5-nm-thick AlN layer that was similar to the electron-blocking layer (EBL) in electrically injected UV lasers and served as a protection layer in the optically pumped lasers. Details regarding the growth can be found elsewhere.[11]

To assess the structural properties of the MQW structures, samples were prepared for scanning transmission electron microscopy (STEM) via the Si-stacking procedure.[18] STEM imaging was performed using an FEI G2 60–300 kV Titan operated at 200 kV with a 19.6 mrad convergence angle and a 77 mrad collection semi-angle. A typical STEM image of a sample with an Al content of 65% in the barriers is shown in Fig. 1. All the wells and barriers are homogenous, and the interfaces are sharp and well-defined. For the depicted sample, the Al content in the barriers and waveguide is the same (65%). Band-structure potential fluctuations due to inhomogeneous Al incorporation, as previously observed in AlGaN MQWs grown on SiC and sapphire, are never observed for structures grown on AlN substrates with proper surface supersaturation control.[19–22]

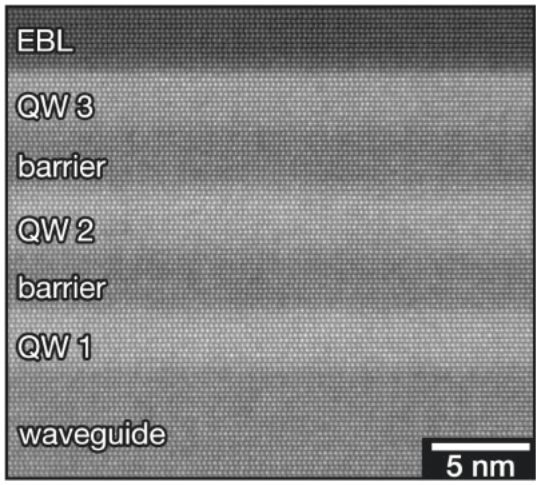

Fig. 1. STEM image of an $Al_{0.55}Ga_{0.45}N/Al_{0.65}Ga_{0.35}N$ MQW structure with an EBL. All wells and barriers are well-defined and of homogenous composition.

After the growth, all samples were thinned and backside-polished to allow for reliable cleaving. The cleaved laser bars were mounted for photoluminescence (PL) and optically pumped laser measurements.[23] An ArF ($\lambda = 193$ nm, $E_{photon} = 6.4$ eV) laser was used as an excitation source. The beam intensity was reduced to a reasonable pumping power using several neutral-density filters and then focused onto the samples. The excitation power was measured using a Coherent Powermax power meter. For optically pumped lasing, light was collected from the cleaved facets of the structures using an optical fiber. Light dispersion and detec-

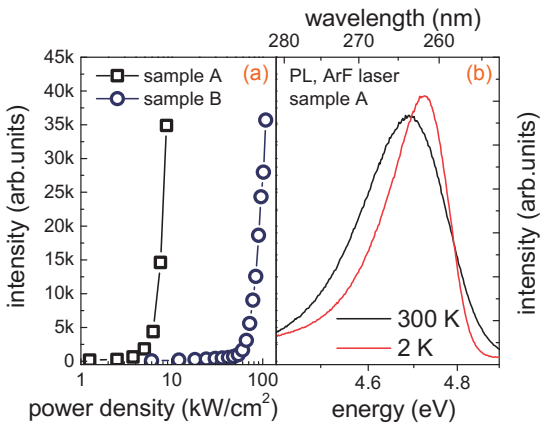

Fig. 2. (a) UV light emission intensity of optically pumped lasers as a function of the excitation power density for a sample with AlN barriers, where the waveguide was grown under high (sample A) and low (sample B) supersaturation. It is found that a lower point defect concentration (sample A) reduces the laser threshold by approximately 1 order of magnitude. (b) Low-temperature (2 K) and room-temperature PL spectra of an AlGaN/AlN MQW (sample A). The room-temperature IQE of the MQW of 95% at a carrier concentration of 1×10^{18} cm^{-3} is estimated according to the temperature-dependent PL data.

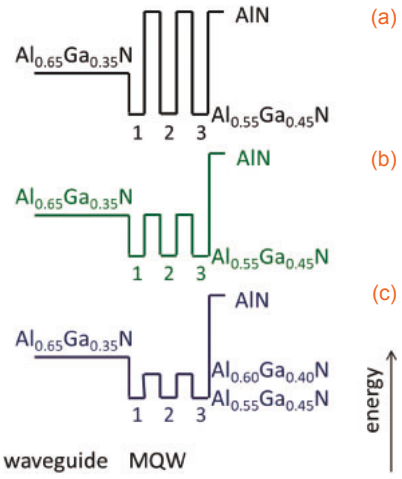

Fig. 3. Schematics of conduction-band structures of three samples with different barrier compositions: (a) barriers with a higher Al content than the waveguide, (b) barriers with the same Al content as the waveguide, and (c) barriers with a lower Al content than the waveguide.

tion was performed using a 0.75-m single monochromator and a cooled charge-coupled device camera.

The effect of the growth conditions on the internal quantum efficiency (IQE) has previously been discussed,[11] showing that an increase in supersaturation via higher V/III ratios led to higher IQEs for a given carrier concentration owing to a decrease in the non-radiative recombination. This demonstrated that in addition to dislocations, point defects were another major factor that strongly influenced the optical quality of AlGaN-based UV lasers. Therefore, to reduce the laser threshold of optically pumped UV lasers, further reduction of point defects in the MQW and the AlGaN waveguide was pursued. Figure 2(a) compares the laser threshold of an optically pumped laser where the waveguide and MQW were grown under V/III ratios of 1,300 (sample A) and 400 (sample B) by varying the ammonia flow rate. This represents high and low supersaturation, respectively. Increasing the supersaturation by increasing the V/III ratio is expected to reduce the point defect concentration and the non-radiative recombination in sample A.[11,24,25]

Both laser structures emitted light at 267 nm. From Fig. 2(a), it is found that both samples show the typical laser turn-on behavior that is expected for optically pumped lasing.[3] In addition, a reduction in the full width at half maximum (FWHM) of the emission peak to approximately 1 nm and 100% transverse-electric polarization of the emitted light was observed above the laser threshold. However, it is found that the sample with the lower point defect concentration (sample A) has a threshold of 6 kW/cm^2, which is a reduction of 1 order of magnitude compared with sample B (60 kW/cm^2). Figure 2(b) shows room-temperature and low-temperature (2 K) PL spectra for sample A. When the temperature is increased from 2 K to room temperature, the intensity of the MQW emission is only slightly reduced. According to the observed intensity reduction, the IQE of the MQW is determined to be 95% at an estimated carrier density of 1×10^{18} cm^{-3} (50 kW/cm^2). This result was confirmed using power-dependent IQE measurements and is a major improvement over previously reported values.[11] In contrast, sample B showed a significantly more drastic drop of the light intensity under the same illumination condition (not shown). At 1×10^{18} cm^{-3} (50 kW/cm^2), this sample exhibited only 2/3 of the IQE of sample A, which agrees well with previous results.[11] Both the IQE and laser threshold measurements confirm that point defects have a significant impact on the performance of MQWs and therefore UV light-emitting diodes and lasers. It is noted that the impact of the point defects on the laser threshold is more pronounced than the impact on the IQE. It is argued that this is because point defects not only impact the free carriers and generation of light via radiative recombination but also cause optical loss/modal loss via absorption of the laser light waves. This has recently been investigated experimentally and theoretically for UV laser devices.[26] Finally, it should be pointed out that a reduction of the point defect concentration can be achieved using tools besides the V/III ratio, including supersaturation (temperature, carrier gas, pressure, etc.) or external measures such as Fermi-level control.[24,27]

On the basis of the low-point defect density sample A, a series of MQWs with varying Al content in the barriers was grown to investigate the influence of the barrier composition in the MQW on the carrier recombination and emission properties. Figure 3 shows schematics of the conduction band structures of samples with AlN barriers (a), as well as AlGaN barriers with Al contents of 65% (b) and 60% (c). Because the waveguide composition was 65% Al, the first sample had barriers with a higher Al content than the waveguide, the barriers for the second sample had the same Al content as the waveguide, and the third sample had a lower Al content in the barriers than that in the waveguide.

In room-temperature PL measurements, all samples exhibited a strong emission around 265 nm. The FWHM of the PL emission peaks at room temperature was approximately 12 nm. When luminescence was collected from the cleaved facets, optically pumped lasing was observed for all samples. However, different excitation power densities were needed to achieve lasing, depending on the Al content in the barriers. Figure 4 shows the emission intensity of the MQW

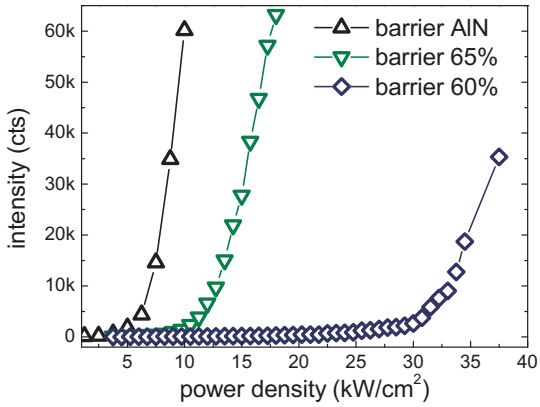

Fig. 4. Emission intensity of three different MQW structures as a function of the excitation power density. The laser threshold increases with the decreasing barrier height.

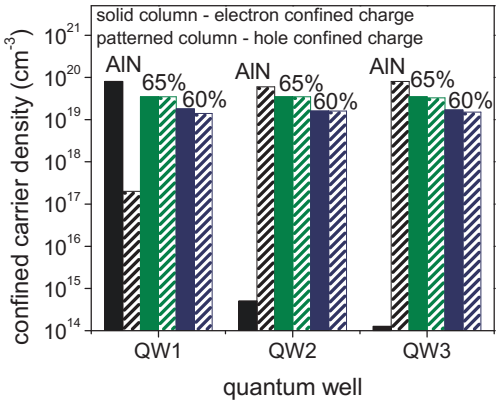

Fig. 5. Electron and hole density (solid bars and striped bars, respectively) in the three AlGaN QWs with different barriers. For the AlN barriers (black bars), electrons are found only in the first QW, while the use of AlGaN barriers (green and blue bars) leads to sufficient electron and hole injection into all three QWs. The laser structure was simulated using the ATLAS framework (SILVACO).

peaks as a function of the excitation power density for the three different barrier configurations. All three samples show clear lasing threshold behavior with a well-defined nonlinear intensity increase above the threshold. The sample with the lowest threshold is the same as sample A in Fig. 2. Comparing the threshold of the different lasers reveals a clear trend towards a lower threshold for higher barriers. Accordingly, the highest threshold is observed for the sample with an Al content of 60% in the barriers (32 kW/cm^2), which is approximately five times higher than the threshold of the sample with AlN barriers (6 kW/cm^2). The structure with 65% Al in the AlGaN barriers has a threshold of 11 kW/cm^2. Because the wells in the investigated MQWs are relatively thin (2.5 nm), some leakage of the electron and hole wave function into the barriers can be expected.[28] This leakage is reduced if the Al content in the barriers is increased. Therefore, the origin of the difference in the threshold is likely the better confinement of carriers in the wells surrounded by higher barriers, leading to lower leakage into the barriers. Other factors that may contribute to the improved performance include the material gain, oscillator strength, and carrier lifetime. Lastly, it should be mentioned that even for the lasers with the lowest barriers, the threshold is significantly better than that of the structures with a higher point defect concentration (sample B in Fig. 2), which highlights the need for clean epitaxial layers. This demonstrates that to achieve electrically injected UV lasers, control of the epitaxy and reduction of defects are required before the optimization of the device structure.

The experimental data clearly indicate that AlN barriers are advantageous for improving the carrier confinement and reducing the lasing threshold for optically pumped lasers. However, optically pumped lasing does not consider carrier injection into the MQW under conditions important for electrically injected UV laser diodes. This is demonstrated by data obtained from the simulation (ATLAS) of complete laser structures (700 nm n-cladding/60 nm n-waveguide/MQW/60 nm p-waveguide/60 nm p-cladding/p-GaN–the Al-content in the cladding layers is 70% and in the waveguide is 65%). As an example, Fig. 5 shows the number of confined electrons (solid columns) and holes (striped columns) in the active region of a laser diode with three wells separated by AlN barriers (black), AlGaN barriers with an Al content of 65% (green), and AlGaN barriers with an Al content of 60% (blue). The applied voltage in all three cases was kept constant. In the structure with the AlN barriers, the electrons are injected primarily into QW1 (QW adjacent to the n-doped waveguide), and the holes are injected into QW3 (QW adjacent to the p-doped waveguide). Insufficient electron injection is predicted for the simulated device with the AlN barriers. While the electron concentration in QW1 (black solid bar) is on the order of 10^{20} cm^{-3}, in QW2, the concentration has already dropped below 10^{15} cm^{-3}. The predictions for the hole injection are slightly better; however, a drop of 3 orders of magnitude is observed when QW3 and QW1 are compared. This drop in the carrier concentration is due to the significant conduction-band and valence-band offset between AlN and AlGaN with 65% Al.[29] Thus, it becomes obvious that because the conduction- and valence-band offsets in the AlGaN heterojunctions are split roughly 2/3 and 1/3 of the bandgap difference,[29,30] AlN acts as a very effective EBL. Consequently, to increase the carrier injection into MQWs for UV lasers, AlGaN barriers are mandatory. As shown in Fig. 5, neither hole nor electron injection should be a significant challenge in AlGaN/AlGaN-based MQWs if the composition contrast between the wells and barriers is approximately 10%, which results in approximately 200- and 100-meV barriers for the electrons and holes, respectively. A lower contrast results in poorer carrier confinement but a more uniform carrier distribution across all three QWs, as shown in Fig. 5.

In summary, we investigated the influence of point defects and the MQW design on the optical and electrical properties of UV laser structures. A low optically pumped laser threshold of 6 kW/cm^2 was found for AlGaN-based MQWs with AlN barriers. A 1 order of magnitude decrease in the lasing threshold compared with the literature data was achieved by controlling the point defects in the MQW and in the underlying waveguide. The V/III ratio is only one pathway for reducing the point defect-concentration in devices. Others include supersaturation (temperature, carrier gas, pressure, etc.) and external control, such as Fermi-level control.[24,27] For barriers with a lower Al-content, a slightly increased laser threshold was observed. This observation is explained by the

better carrier confinement under optical pumping for the MQWs with high barriers. Maximization of the carrier confinement is consistent with the design of optically pumped laser structures. However, for electrically driven lasers, carrier injection into MQWs with AlN barriers is insufficient owing to the significant band offset between the AlN and AlGaN with 55% Al, and it is necessary to use lower barriers to ensure sufficient carrier injection into all QWs. Lowering of the barriers increases the threshold, as discussed previously. However, Figs. 4 and 5 show that the effect is marginal.

Acknowledgments The authors acknowledge partial financial support from ARL (W56KGU-15-C-0052, W56KGU-14-C-0046), NSF (ECCS-1508854, ECCS-1610992, DMR-1508191, ECCS-1653383), and ARO (W911NF-15-2-0068, W911NF-16-C-0101). Part of this work was performed at the Analytical Instrumentation Facility (AIF) of North Carolina State University, which is supported by the State of North Carolina and the National Science Foundation (award number ECCS-1542015). The AIF is a member of the North Carolina Research Triangle Nanotechnology Network (RTNN), which is a site in the National Nanotechnology Coordinated Infrastructure (NNCI).

1) M. Kneissl, in *III–Nitride Ultraviolet Emitters: Technology and Applications*, ed. M. Kneissl and J. Rass (Springer, Cham, 2016) Chap. 1.
2) R. Kirste, N. Rohrbaugh, I. Bryan, Z. Bryan, R. Collazo, and A. Ivanisevic, Annu. Rev. Anal. Chem. **8**, 149 (2015).
3) J. Xie, S. Mita, Z. Bryan, W. Guo, L. Hussey, B. Moody, R. Schlesser, R. Kirste, M. Gerhold, R. Collazo, and Z. Sitar, Appl. Phys. Lett. **102**, 171102 (2013).
4) T. Wunderer, C. L. Chua, J. E. Northrup, Z. Yang, N. M. Johnson, M. Kneissl, G. A. Garrett, H. Shen, M. Wraback, B. Moody, H. S. Craft, R. Schlesser, R. F. Dalmau, and Z. Sitar, Phys. Status Solidi C **9**, 822 (2012).
5) F. Asif, M. Lachab, A. Coleman, I. Ahmad, B. Zhang, V. Adivarahan, and A. Khan, J. Vac. Sci. Technol. B **32**, 061204 (2014).
6) X.-H. Li, T. Detchprohm, T.-T. Kao, M. M. Satter, S.-C. Shen, P. D. Yoder, R. D. Dupuis, S. Wang, Y. O. Wei, H. Xie, A. M. Fischer, F. A. Ponce, T. Wernicke, C. Reich, M. Martens, and M. Kneissl, Appl. Phys. Lett. **105**, 141106 (2014).
7) J. Zhang, H. Zhao, and N. Tansu, Appl. Phys. Lett. **98**, 171111 (2011).
8) Y.-S. Liu, Z. Lochner, T.-T. Kao, M. M. Satter, X.-H. Li, J.-H. Ryou, S.-C. Shen, P. D. Yoder, T. Detchprohm, R. D. Dupuis, Y. Wei, H. Xie, A. Fischer, and F. Ponce, Phys. Status Solidi C **11**, 258 (2014).
9) D. Li, K. Jiang, X. Sun, and C. Guo, Adv. Opt. Photonics **10**, 43 (2018).
10) H. Amano, J. Phys.: Conf. Ser. **326**, 012002 (2011).
11) Z. Bryan, I. Bryan, J. Xie, S. Mita, Z. Sitar, and R. Collazo, Appl. Phys. Lett. **106**, 142107 (2015).
12) M. Shatalov, W. Sun, A. Lunev, X. Hu, A. Dobrinsky, Y. Bilenko, J. Yang, M. Shur, R. Gaska, C. Moe, G. Garrett, and M. Wraback, Appl. Phys. Express **5**, 082101 (2012).
13) W. W. Chow, M. Kneissl, J. E. Northrup, and N. M. Johnson, Appl. Phys. Lett. **90**, 101116 (2007).
14) S. Nakamura, S. Pearton, and G. Fasol, *The Blue Laser Diode: The Complete Story* (Springer, Berlin, 2013).
15) R. Dalmau, B. Moody, R. Schlesser, S. Mita, J. Xie, M. Feneberg, B. Neuschl, K. Thonke, R. Collazo, A. Rice, J. Tweedie, and Z. Sitar, J. Electrochem. Soc. **158**, H530 (2011).
16) A. Rice, R. Collazo, J. Tweedie, R. Dalmau, S. Mita, J. Xie, and Z. Sitar, J. Appl. Phys. **108**, 043510 (2010).
17) D. Ehrentraut and Z. Sitar, MRS Bull. **34**, 259 (2009).
18) J. H. Dycus and J. M. Lebeau, J. Microsc. **268**, 225 (2017).
19) E. F. Pecora, W. Zhang, A. Y. Nikiforov, L. Zhou, D. J. Smith, J. Yin, R. Paiella, L. D. Negro, and T. D. Moustakas, Appl. Phys. Lett. **100**, 061111 (2012).
20) Y. Iwata, T. Oto, D. Gachet, R. G. Banal, M. Funato, and Y. Kawakami, J. Appl. Phys. **117**, 115702 (2015).
21) I. Bryan, Z. Bryan, S. Mita, A. Rice, J. Tweedie, R. Collazo, and Z. Sitar, J. Cryst. Growth **438**, 81 (2016).
22) I. Bryan, Z. Bryan, S. Mita, A. Rice, L. Hussey, C. Shelton, J. Tweedie, J.-P. Maria, R. Collazo, and Z. Sitar, J. Cryst. Growth **451**, 65 (2016).
23) W. Guo, Z. Bryan, J. Q. Xie, R. Kirste, S. Mita, I. Bryan, L. Hussey, M. Bobea, B. Haidet, M. Gerhold, R. Collazo, and Z. Sitar, J. Appl. Phys. **115**, 103108 (2014).
24) F. Kaess, S. Mita, J. Xie, P. Reddy, A. Klump, L. H. Hernandez-Balderrama, S. Washiyama, A. Franke, R. Kirste, A. Hoffmann, R. Collazo, and Z. Sitar, J. Appl. Phys. **120**, 105701 (2016).
25) P. Reddy, F. Kaess, J. Tweedie, R. Kirste, S. Mita, R. Collazo, and Z. Sitar, Appl. Phys. Lett. **111**, 152101 (2017).
26) M. Martens, C. Kuhn, T. Simoneit, S. Hagedorn, A. Knauer, T. Wernicke, M. Weyers, and M. Kneissl, Appl. Phys. Lett. **110**, 081103 (2017).
27) S. Mita, R. Collazo, A. Rice, R. F. Dalmau, and Z. Sitar, J. Appl. Phys. **104**, 013521 (2008).
28) K. Kojima, K. Furusawa, Y. Yamazaki, H. Miyake, K. Hiramatsu, and S. F. Chichibu, Appl. Phys. Express **10**, 015802 (2017).
29) P. Reddy, I. Bryan, Z. Bryan, J. Tweedie, S. Washiyama, R. Kirste, S. Mita, R. Collazo, and Z. Sitar, Appl. Phys. Lett. **107**, 091603 (2015).
30) Z. Sitar, M. J. Paisley, B. Yan, R. F. Davis, J. Ruan, and J. W. Choyke, Thin Solid Films **200**, 311 (1991).